Fluctuation-induced flux at the plasma edge in toroidal devices

B. A. Carreras
Oak Ridge National Laboratory, Oak Ridge, Tennessee 37831-8070

C. Hidalgo, E. Sánchez, M. A. Pedrosa, R. Balbín, I. García-Cortés, and B. van Milligen
Asociación Euratom-Ciemat, 28040 Madrid, Spain

D. E. Newman and V. E. Lynch
Oak Ridge National Laboratory, Oak Ridge, Tennessee 37831-8070

Fluctuation-induced fluxes have a bursty character. As a consequence, a significant part of the total particle flux is carried out by sporadic, large transport bursts. The local flux distribution function is consistent with a near-Gaussian character of the fluctuations. The radial dependence of the statistical properties of plasma fluctuations and induced fluxes have been investigated in the plasma boundary region of the TJ-I tokamak [I. García-Cortés *et al.*, Phys. Fluids B **4**, 4007 (1992)] and the TJ-IU torsatron [E. Ascasibar *et al.*, in *Plasma Physics and Controlled Fusion Research*, Proceedings of the 15th Conference on Plasma Physics and Controlled Nuclear Fusion Research, Seville (International Atomic Energy Agency, Vienna, in press)]. There is a striking similarity between the statistical properties of turbulent transport in both devices. © *1996 American Institute of Physics.* [S1070-664X(96)04407-2]

I. INTRODUCTION

To improve our understanding of edge plasma turbulence, comparative studies of the structure of the turbulence in tokamaks, stellarators, and reversed-field pinch devices have been carried out in the last few years.[1–3] A reversal in the phase velocity of the fluctuations (shear layer) has been seen in the plasma boundary region in tokamaks and stellarators.[1,4,5] The shear layer location determines a characteristic plasma radius[6] and provides a convenient way to compare the structure of the fluctuations in different magnetic confinement devices.

The overall similarity in the structure of the turbulence for currentless plasmas [such as those in the Advanced Toroidal Facility[7] (ATF)] and tokamak plasmas [such as in the Texas Experimental Tokamak[8] (TEXT)] suggests that plasma current and applied toroidal electric field are not the dominant drive for turbulence in the plasma boundary region.[1] A detailed comparison of the spatial and temporal correlation functions of the scrape-off layer (SOL) turbulence[9] in the Axially Symmetric Divertor Experiment (ASDEX)[10] tokamak and the Wendelstein 7 Advanced Stellarator[11] (W7-AS) has been reported; in both devices the turbulence shares the same basic properties.[3]

In order to delve deeper into the mechanisms underlying turbulent transport, it is important to measure not only the fluctuation-induced transport, which can account for most of the particle transport in the plasma edge region in tokamaks and stellarators, but also the statistical properties of the time-resolved turbulent flux.[12]

In this paper, we study the statistical properties of plasma fluctuations and induced particle flux in the TJ-I tokamak[13] and TJ-IU torsatron.[14] We have carried out comparative studies of the statistical properties of the turbulent transport in both devices. The experimental results have also been compared with predictions from different turbulence models. Gaussian fluctuations induce bursty turbulent fluxes.

Therefore, the near-Gaussian character of the measured fluctuations is probably responsible for the bursty character of the experimentally determined fluxes.

The remainder of this paper is organized as follows. In Sec. II, the experimental setup for the measurement of the turbulent flux is described and its statistical properties are presented in Sec. III. Section IV is dedicated to the interpretation of the experimental results, and they are compared to theoretical models in Sec. V. The variation of the local flux probability distribution function (PDF) with radial position is discussed in Sec. VI, and the conclusions are presented in Sec. VII.

II. EXPERIMENTAL SETUP FOR THE TURBULENT FLUX MEASUREMENTS

The time-resolved radial turbulent flux, $\Gamma_T = \tilde{n}\tilde{E}_\theta/B_T$, has been measured in the plasma boundary region in the TJ-I tokamak[13] and in the TJ-IU torsatron.[14] Here $\tilde{n}$ and $\tilde{E}_\theta$ are the fluctuating electron density and poloidal electric field, respectively, and B_T the toroidal magnetic field. The turbulent flux is measured by means of Langmuir probes and by using the experimental technique described in Ref. 6. The Ohmically heated TJ-I plasmas are characterized by a major radius $R = 30$ cm, minor radius $a = 10$ cm, plasma current $I_p \approx 30$ kA, toroidal field $B_T \approx (1.0–1.4)$ T, and density $n_e \approx (1-3) \times 10^{13}$ cm^{-3}. Around the velocity shear location, the electron temperature is about $T_e \approx 30$ eV with electron densities in the range $n_e \approx (1-2) \times 10^{12}$ cm^{-3}. The TJ-IU electron cyclotron resonance heated (ECRH) plasmas are characterized by $R = 60$ cm, the central rotational transform $\iota(0) \approx 0.21$, the averaged minor radius $\hat{a} = 10$ cm, $B_T \approx 0.6$ T, and $n_e \approx 0.5 \times 10^{13}$ cm^{-3}. At the velocity shear layer $T_e \approx 20$ eV and $n_e \approx (0.5-1) \times 10^{12}$ cm^{-3}.

A probe with three tips is used in these measurements. Two of the tips are aligned perpendicular to the magnetic field and poloidally separated by a distance of $\Delta = 0.2$ cm.
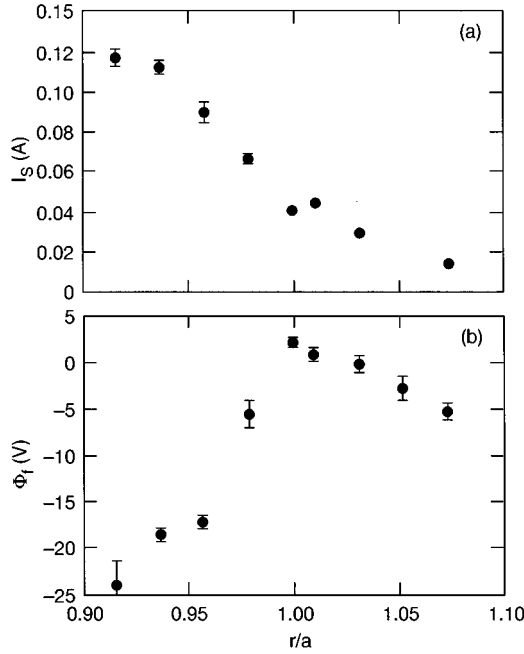
FIG. 1. Plasma profiles of the ion saturation current (I_s) and floating potential (Φ_f) in the plasma boundary region in the TJ-I tokamak.

They are used to measure the fluctuating poloidal electric field by measuring the floating potential fluctuations, $\tilde{\Phi}_f$, at two poloidal positions, $\tilde{E}_\theta = [\tilde{\Phi}_f(\theta_1) - \tilde{\Phi}_f(\theta_2)]/\Delta$. All fluctuating quantities are indicated by a tilde and are defined as having zero time-averaged value; thus, $\langle \tilde{E}_\theta \rangle = 0$. From this two-pin measurement, we can also infer the poloidal phase velocity of the fluctuations. The third tip of the probe is located between the other two, but at a slightly displaced radius. It is biased at a fixed voltage in the ion saturation regime to measure electron density fluctuations; we assume that $\tilde{n} \propto \tilde{I}_s$ where I_s is the ion saturation current.

The statistical properties of the radial particle flux Γ_T has been computed from the measured values of the ion saturation and floating potential fluctuations with the electron temperature ($\tilde{T}_e$) effects being neglected.[15] The turbulent flux has been measured both in the plasma edge ($r < a_s$) and in the scrape-off layer ($r < a_s$), where a_s is the radial location of the velocity shear layer.

In Fig. 1, typical radial profiles of the ion saturation current (I_s) and floating potential (Φ_f) in the plasma boundary region of the TJ-I tokamak are shown. The velocity shear layer location has been used as a point of reference.[13] The time evolution of the normalized turbulent radial flux measured in the proximity of the velocity shear layer is shown in Fig. 2. As in other devices,[12,16,17] the flux is predominantly positive (i.e., the particle transport is, on average, outward) and bursty. This temporal behavior of the turbulent particle flux is typical of all measurements carried out in TJ-I and TJ-IU, and to better understand its significance, we perform a statistical analysis of the local flux measurements.

III. STATISTICAL PROPERTIES OF THE MEASURED FLUCTUATION-INDUCED FLUXES

In order to carry out the statistical analysis, we calculate the local flux PDF. The PDF of the time-resolved normalized
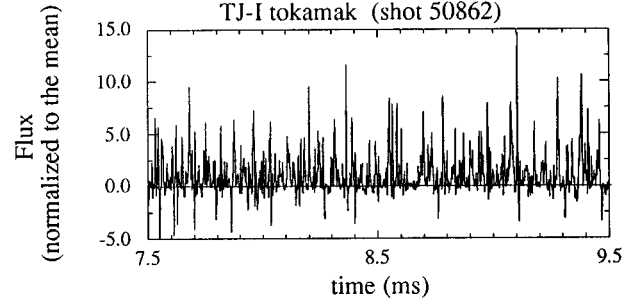

FIG. 2. Time evolution of the turbulent particle flux in TJ-I tokamak measured in the proximity of the velocity shear layer location.

turbulent flux, $\Gamma_n \equiv \Gamma_T(t)/\langle \Gamma_T(t) \rangle$ (i.e., the time-resolved local flux normalized to its mean value), is calculated by

$$p(\Gamma_n) = \frac{N_{\Gamma_n}}{N}. \tag{1}$$

For each time sample, N_{Γ_n} is the number of values of Γ_n that fall within the range $\Gamma_n \pm W/2$, where W is the length of an interval centered at Γ_n and N is the total number of data points in the sample. Typically the value of Γ_n is in the range -20 to 20; hence, to calculate $p(\Gamma_n)$, the full range of Γ_n values (from -20 to $+20$) has been divided into 80 intervals of equal length ($W = 0.5$). The number of data values in each class interval has been tabulated and divided by the sample size. Because of the bursty behavior of the flux, it is also interesting to evaluate the fraction of the total flux carried out by the large bursts. To do so, we calculate the flux fraction function defined as $F_F(\Gamma_n) = p(\Gamma_n) \times \Gamma_n$.

The local flux PDF is not symmetric. This asymmetry gives a measure of the average flux out compared to the maximum instantaneous fluxes. To quantify these properties of the PDF, we also calculate the skewness (S) and the kurtosis (K), that is, third and fourth order moments of the PDF, respectively. We use the same interval of amplitudes (± 20) and the expressions

$$S = \langle [\Gamma_n(t) - \langle \Gamma_n \rangle]^3 \rangle / \sigma^3, \tag{2}$$

and

$$K = \langle [\Gamma_n(t) - \langle \Gamma_n \rangle]^4 \rangle / \sigma^4. \tag{3}$$

Here, σ is the standard deviation. In these evaluations, the accuracy of these higher moments of the PDF is a serious question. We will discuss later other ways of documenting the asymmetry of the local flux PDF.

The local flux PDF at different radial locations is shown in Fig. 3(a). The PDF has a clear non-Gaussian character. The corresponding flux fraction function is plotted in Fig. 3(b). There are large amplitude transport bursts that account for a significant part of the total flux. To quantify this effect, let us calculate the fraction of the flux carried by flux events equal to or larger than a given Γ_n:

$$F_{>\Gamma_n} = \int_{\Gamma_n}^{\infty} d\Gamma_n' \, p(\Gamma_n') \Gamma_n'. \tag{4}$$
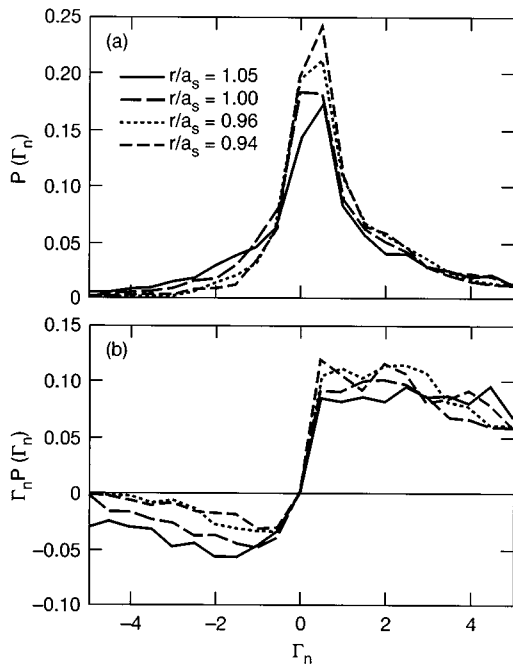
FIG. 3. Experimental measurement of particle flux at the plasma edge in TJ-I at different radial positions: (a) local flux PDF and (b) flux fraction function.

We plotted the probability of such flux events versus the fraction of the flux in Fig. 4 for a typical shot in TJ-I. For instance, we can see from this plot that 10% of the largest flux events carry out 50% of the averaged particle flux, giving a measure of the intermittent character of the flux. In this figure, the fraction of the flux goes above 1 because there are also inward flux events.

The form of the local flux PDF seems to be quite general. In Fig. 5(a), we have plotted the local flux PDF for TJ-I and TJ-IU plasmas. Measurement were taken in the plasma edge region ($r < a_s$). The fraction of transport as a function of the normalized flux is shown in Fig. 5(b). There is a striking similarity between the local flux PDF in both devices. This result is particularly interesting in view of the strong differences between TJ-I and TJ-IU plasmas. Furthermore, in both devices a significant fraction of the total flux can be attributed to the presence of large sporadic bursts. Therefore,
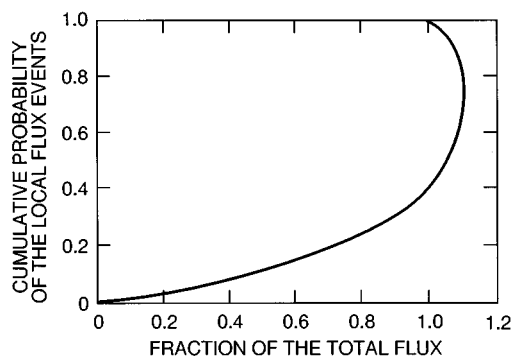

FIG. 4. Cumulative probability of flux events that carry a given fraction of the averaged particle flux.
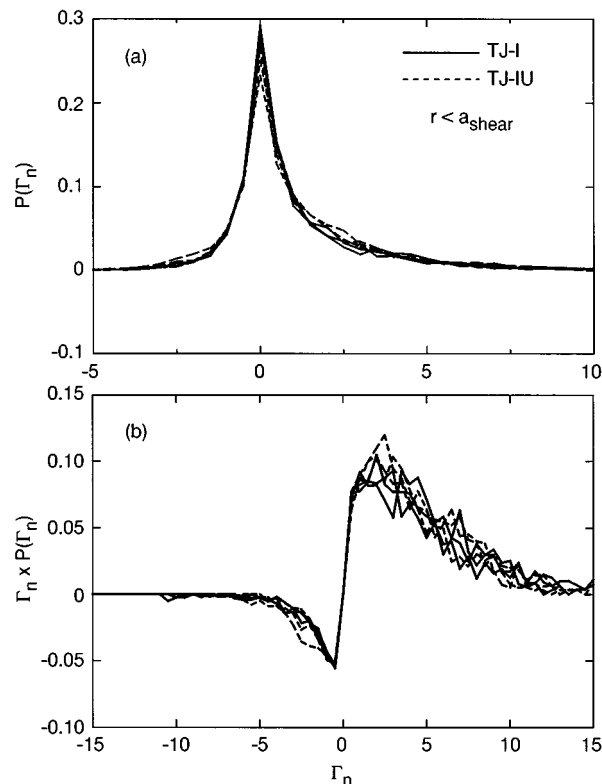

FIG. 5. Comparison of the statistical properties of turbulent transport in the plasma edge region ($r < a_s$) in the TJ-I tokamak and TJ-IU torsatron: (a) distribution function and (b) flux fraction function versus flux (normalized to the mean).

the local transport has an intermittent character. The comparison between TJ-I and TJ-IU suggests that the statistical properties of turbulent fluxes are not determined by plasma parameters like plasma current, magnetic shear, plasma density, or magnetic field.

To do more detailed comparisons between PDFs, it is useful to introduce a variant of the quantile–quantile plots.[18] These plots are constructed in the following way. If f_1 and f_2 are the two distribution functions to compare, we calculate the corresponding cumulative PDFs, F_1 and F_2, as

$$F_i(\Gamma) = \int_{-\infty}^{\Gamma} d\Gamma' \, f_i(\Gamma'), \quad i = 1, 2, \tag{5}$$

and plot $\Delta F \equiv F_1 - F_2$ vs F_1. These types of plots allow us to apply directly the Kolmogorov (for an analytical versus a numerical PDF) and Smirnov (between two numerical PDFs) goodness-of-fit tests[18] and, at the same time, to distinguish between statistical and systematic differences between PDFs. If we know the theoretical form of the PDF, when we compare it with the experiment, the quantile–quantile plot should show scattered points; that is, the difference between the theory and the data should be due to statistical noise. However, if the plot shows a continuous function, it indicates that the theoretical PDF probably does not give a good description of the experiment. Possibly, the functional form is not right and the differences are not statistical but systematic. To test if that is the case, we repeat the plot with half of the statistical sample and test whether the deviation has the same
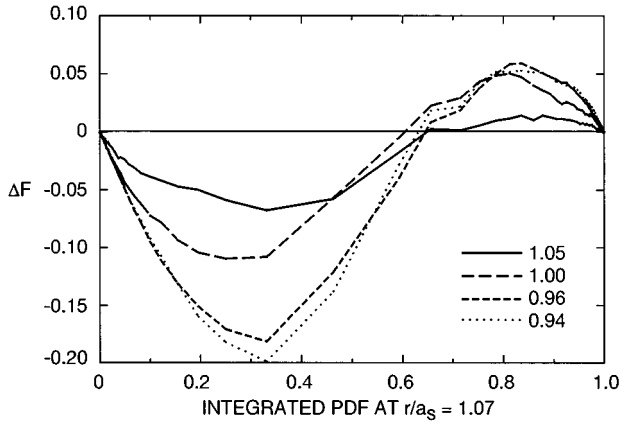
FIG. 6. Quantile–quantile plot for the local flux PDFs of the radial scan, all referred to the PDF at $r/a_s = 1.07$.

FIG. 7. Local flux PDF as calculated from Eq. (7) for $\gamma = 0.5$, -0.5, and -0.2.

dependence regardless of the statistics. This type of test has proven very valuable in comparing PDFs. An example is given in Fig. 6, where we have plotted the deviation of the distribution functions at different radial positions with respect to the PDF at $r/a_s = 1.07$. These data have the same sequence of PDFs as in Fig. 3. However, Fig. 6 shows that the change in the PDFs with radius is a systematic change, not a difference due to statistical errors. Hereafter, we will use these plots to compare PDFs and to separate statistical from systematic effects.

IV. INTERPRETATION OF THE PDF OF THE LOCAL PARTICLE FLUX

The functional form of the local flux PDF does not necessarily imply a non-Gaussian character of the fluctuations, on the contrary, it can be interpreted as a consequence of the nearly Gaussian nature of the fluctuations. To see this, let us consider two fluctuating fields, $\tilde{n}$ and $\tilde{V}_r = (1/rB)(\partial \tilde{\Phi}/\partial \theta)$ with Gaussian statistics, but correlated. Here, $\tilde{V}_r$ is the radial velocity fluctuation. If the electrostatic potential fluctuation, $\tilde{\Phi}$, is Gaussian, its derivative with respect to the poloidal angle is also Gaussian. Therefore, we assume that $\tilde{V}_r$ is Gaussian. The PDF for the two-field system is

$$f(\tilde{n}, \tilde{V}_r) = \frac{1}{2\pi} \frac{\sqrt{1-\gamma^2}}{W_V W_n} \exp\left[-\left(\frac{\tilde{V}_r^2}{2W_V^2} + \frac{\tilde{n}^2}{2W_n^2} + \gamma \frac{\tilde{n}\tilde{V}_r}{W_V W_n} \right) \right],$$ (6)

where γ measures the strength and the sign of the correlation between density and velocity fluctuations ($|\gamma| < 1$). The parameters W_n and W_V are the square root of the variances of $\tilde{V}_r$ and $\tilde{n}$, respectively, in the absence of correlation. From Eq. (6), we find that the PDF for the fluctuation-induced turbulent flux, $\Gamma_T = \tilde{n}\tilde{V}_r$, is

$$p(\Gamma_T) = \frac{1}{\pi} \frac{\sqrt{1-\gamma^2}}{W_V W_n} K_0\left(\frac{|\Gamma_T|}{W_V W_n} \right) \exp\left(-\gamma \frac{\Gamma_T}{W_V W_n} \right).$$ (7)

The K_0 is the modified Bessel function, and its argument is symmetric with respect to the direction of the flux. The ex-
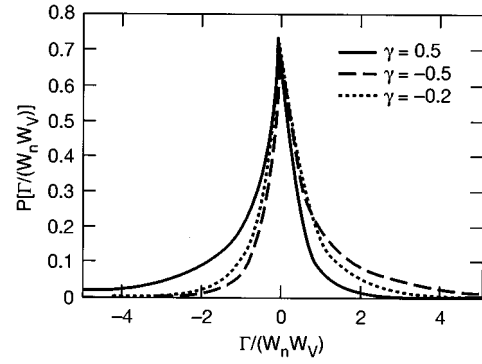
ponential factor breaks the $\Gamma_T \rightarrow -\Gamma_T$ symmetry. This factor takes into account the relative phase between the density and velocity fluctuations. From Eq. (7), the averaged flux is

$$\langle \Gamma \rangle = -\frac{\gamma}{1-\gamma^2} W_n W_V.$$ (8)

For the averaged flux to be outward, $\gamma < 0$. By measuring experimentally the $\tilde{n}$ and $\tilde{V}_r$ PDFs, we can determine W_n and W_V, respectively. Then, the PDF of the local flux gives the correlation parameter γ.

The functional dependence of the local flux PDF given by Eq. (7) is very similar to the experimentally measured one (Fig. 3). In Fig. 7, we have plotted the flux PDF for three different values of γ. The figure shows the similarity with the experimental results and how the direction of the averaged flux changes by changing the sign of γ. For this model, the rms values of the fluctuating fields are

$$\langle \tilde{V}_r^2 \rangle = W_V^2 \frac{1}{1-\gamma^2} \quad \text{and} \quad \langle \tilde{n}^2 \rangle = W_n^2 \frac{1}{1-\gamma^2}.$$ (9)

Therefore, the relative phase α between $\tilde{n}$ and $\tilde{V}_r$ is given by

$$\cos \alpha \equiv \frac{\langle \tilde{V}_r \tilde{n} \rangle}{\langle \tilde{V}_r^2 \rangle^{1/2} \langle \tilde{n}^2 \rangle^{1/2}} = -\gamma.$$ (10)

Therefore, γ is an indirect measure of the relative phase between $\tilde{n}$ and $\tilde{V}_r$. For fluctuations with Gaussian statistics, the parameter γ contains the information on the dynamics and determines all the moments of the PDF. In particular, the variance is

$$\langle (\Gamma - \langle \Gamma \rangle)^2 \rangle = (W_V W_n)^2 \frac{1+\gamma^2}{(1-\gamma^2)^2}.$$ (11)

The skewness of the local flux PDF is

$$S = -2\gamma \frac{3+\gamma^2}{(1+\gamma^2)^{3/2}}.$$ (12)

As the correlation parameter γ varies between -1 and 1, S varies between 2.83 and -2.83. The fourth-order moment, the kurtosis, is

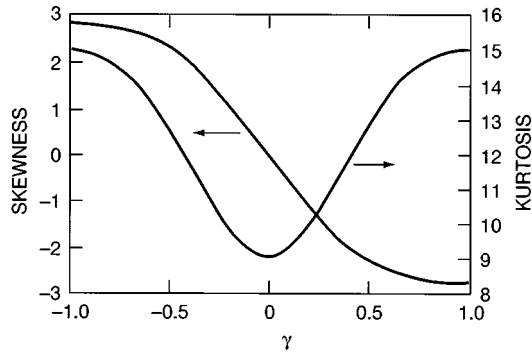$$K = 3 \frac{3+14\gamma^2+3\gamma^4}{(1+\gamma^2)^2},$$ (13)

FIG. 8. Skewness and kurtosis for the PDF of Eq. (7) as a function of γ.

and K can vary between 9 and 15. The dependence of both skewness and kurtosis on the parameter γ is shown in Fig. 8.

In comparing Eq. (7) with the PDFs of the experimental data, it is necessary to be careful with the singular behavior of the K_0 function. After choosing a set of intervals for the flux as is done for the experimental data, we can construct an equivalent PDF by integrating Eq. (7) over each one of the bins, in particular, in the two bins around the origin. This step removes the singularity and permits detailed comparisons. In this way and using the functional form of Eq. (7), we can obtain good fits of the experimental PDFs by chi-square minimization. To test whether the theoretical PDF is a reliable representation of the experimental PDF, we use the quantile–quantile plots. An example is shown in Fig. 9. In this figure, we compare the experimental local flux PDF at $r/a_s=0.94$ from the TJ-I radial scan with the theoretical flux PDF for $\gamma=-0.48$. The theoretical PDF gives a good description of the experimental one because the deviation between the two does not show any systematic trend, but it results mostly from statistical errors. The maximum deviation, in this case, is about 0.012. Naturally, we cannot distinguish between high-moment systematic deviations and statistical ones. It is with this caveat that we take the results in Fig. 9 to be dominated by statistical errors. To test the goodness of the fit, we can use the Kolmogorov test. The criterion for rejection of the fit with 5% confidence level is if any deviation is larger than 0.025. Therefore, using this criterion, the fit is acceptable. For the radial scan in TJ-I, the PDF of
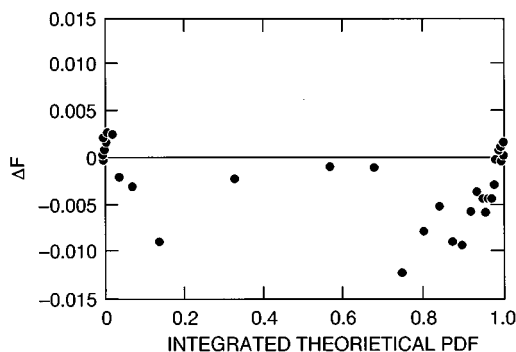

FIG. 9. Quantile–quantile plot for the experimental flux PDF at $r/a_s=0.94$ referred to the theoretical fit using Eq. (7) with $\gamma=0.48$.

Eq. (7) gives an acceptable description of the data except outside the shear layer region. These cases will be discussed in Sec. VI.

V. LOCAL FLUX PDF PREDICTIONS FROM CLASSICAL AND SELF-ORGANIZED CRITICAL TURBULENCE MODELS

We look at the predictions of very different turbulence models in order to find distinguishing features in the predicted flux that could be used for experimental tests. Here we do not discuss the theoretical models because they have been discussed elsewhere. We will focus only on their predictions for the local fluxes.

First, we analyze the results from the modeling[19] of the ATF outer region using resistive pressure-gradient-driven turbulence.[20] The model includes the evolution of the perpendicular and parallel momentum balance equations and the density evolution equation,

$$\frac{\partial \nabla_\perp^2 \tilde{\Phi}}{\partial t} + \mathbf{V} \cdot \nabla \nabla_\perp^2 \tilde{\Phi} = -\frac{1}{\eta m_i n_0 R_0} \nabla_\parallel^2 \tilde{\Phi} + \frac{B_0}{m_i n_0} \frac{T_e}{r_c} \frac{1}{r} \frac{\partial \tilde{n}}{\partial \theta}$$
$$+ \mu \nabla_\perp^4 \tilde{\Phi} \qquad (14)$$

and

$$\frac{\partial \tilde{n}}{\partial t} + \tilde{\mathbf{V}} \cdot \nabla \tilde{n} = \frac{d\langle n \rangle}{dr} \frac{1}{r} \frac{\partial \tilde{\Phi}}{\partial \theta} + \chi_\perp \nabla_\perp^2 \tilde{n}, \qquad (15)$$

respectively, for the fluctuations, and the averaged density evolution is given by

$$\frac{\partial \langle n \rangle}{\partial t} + \frac{1}{r} \frac{\partial}{\partial r} r \langle \tilde{V}_r \tilde{n} \rangle = \chi_\perp \frac{1}{r} \frac{\partial}{\partial r} \left(r \frac{\partial \langle n \rangle}{\partial r} \right), \qquad (16)$$

where $\chi_\perp$ is the collisional diffusivity. Here, the tilde indicates fluctuations and the angled brackets $\langle \ \rangle$ averaged quantities. The toroidal magnetic field is B_0, m_i the ion mass, μ the collisional viscosity, and r_c the radius of magnetic field line curvature.

The three-dimensional nonlinear code KITE[21] was used to advance these equations. These calculations are high-resolution calculations that include 4605 Fourier components, $\Delta r \approx 1/1500$, and they describe the nonlinear interaction of over 1000 different helicities. A problem with the evaluation of statistical quantities from these numerical calculations is the short range of the time samples. To compensate for this, we have used at a fixed time samples of 360 data points at different poloidal angle positions and combined several of these time samples. We have done separate analysis for the L-mode and H-mode phases of the calculation.

The PDF of the fluctuations, both density, $\tilde{n}$, and electrostatic potential, $\tilde{\Phi}$, have Gaussian character within the statistical limitations of the sample. In Fig. 10, we plotted the PDF for electrostatic potential fluctuation at a fixed radius, $r/a=0.76$, and compared it with a Gaussian fit. Because the samples contain only 1080 points, the results are noisy. At all radial positions, the PDFs are equally close to a Gaussian distribution. At the same radial position as the results of Fig. 10, we have calculated the PDF of the particle flux (Fig. 11).
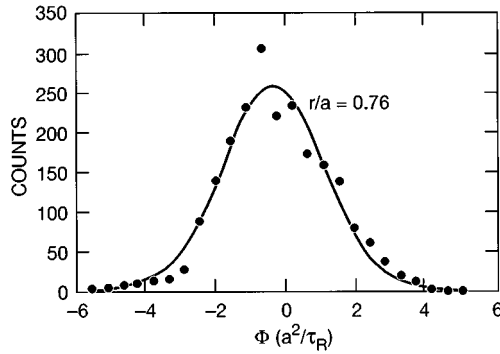
FIG. 10. Electrostatic potential fluctuations PDF from a numerical calculation using resistive pressure-gradient-driven turbulence model.

FIG. 12. Comparison of the local flux PDF in the L- and H-mode states. This is a result from a numerical calculation using resistive pressure-gradient-driven turbulence model.

There is striking similarity between Figs. 3 and 11. The PDF of the local flux obtained in the numerical calculations can be fitted very well with a function of the form of Eq. (7). Similar results were obtained when the radiation-driven drift wave turbulence model[22] was used.

Using the same three-dimensional turbulence model, a transition was triggered by reducing the effective viscosity of the averaged poloidal flow. The objective was to simulate a transition from the low confinement mode (L mode) to the high confinement mode (H mode), although such transition was never observed in ATF. Because of the decreased viscosity, the averaged poloidal flow shear is amplified and the fluctuations change. The fluctuation amplitude is reduced, and the relative phase between density and potential fluctuations modified. However, there is no evidence of a change in the Gaussian character of the fluctuations after the L–H transition. An interesting result of the local flux analysis is obtained by comparing the PDF before and after the transition. There is a significant narrowing of the local flux PDF after the transition. One reason for the change of the PDF is that the averaged rms level of fluctuations has been reduced in the H mode. However, a difference between L- and H-mode PDFs is still present when the fluxes are normalized to their mean value (Fig. 12). In particular, we have obtained $\gamma = 0.42$ for L mode and $\gamma = 0.54$ for the H mode, indicating that not only the level but also the phase of the fluctuations has changed at the transition. This effect has already been ob-
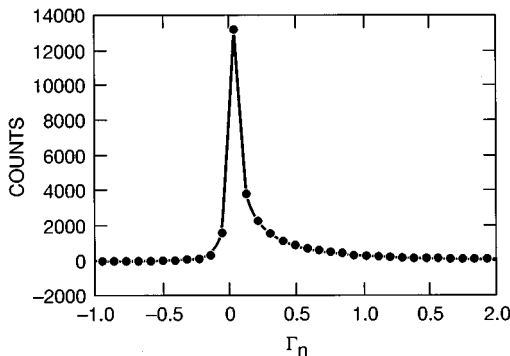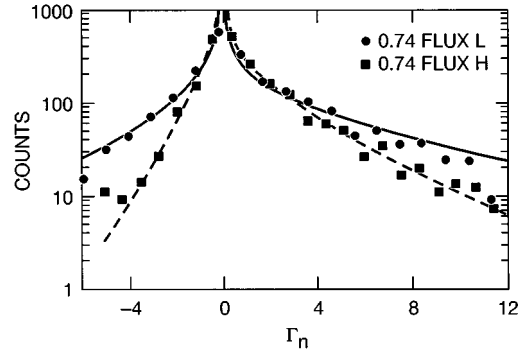
served in our previous calculations[23] and is induced by the sheared flow decorrelation effect.

Models based on self-organized criticality (SOC)[24,25] have, in principle, quite different fluctuation dynamics than the classical turbulence models.[26] The former corresponds to a subcritical state with added noise while for the latter the turbulence is supercritical. The same drive can be used to describe these two types of turbulence dynamics. Hence, we have used the resistive pressure-gradient-driven turbulence model, Eqs. (14) and (15), and relaxed the profile to a SOC state. The average density equation was evolved without collisional diffusivity and with added random noise:

$$\frac{\partial \langle n \rangle}{\partial t} + \frac{1}{r} \frac{\partial}{\partial r} r \langle \tilde{V}_r \tilde{n} \rangle = \tilde{S}. \tag{17}$$

This model leads to transport in a subcritical state: the transport is locally diffusive, and the diffusivity is a fractional power of the noise level. In these calculations, the noise is randomly distributed in radius. In spite of the different dynamics, the PDF of the fluctuations is again close to Gaussian (Fig. 13). Because of the small size of the time samples, the noise level is large. From the Gaussian character of the fluctuations, we can obtain the usual form for the PDF of the local flux.

Using the sandpile analog for SOC transport,[26] we can accumulate large data samples. In this case, we calculate the

FIG. 11. Local flux PDF from a numerical calculation using resistive pressure-gradient-driven turbulence model.
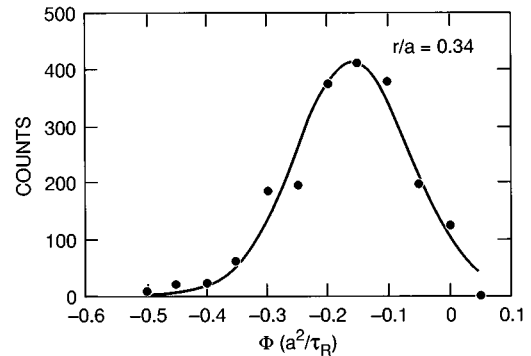

FIG. 13. Electrostatic potential fluctuations PDF from a numerical calculation based on a model realization of a self-organized criticality.
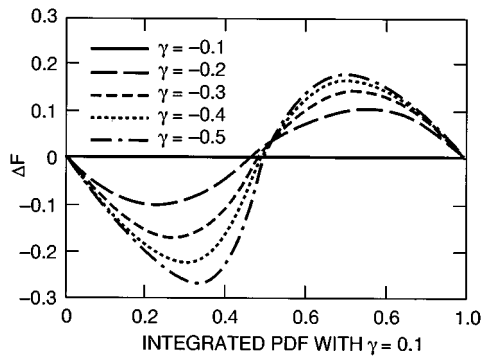
FIG. 14. Quantile–quantile plot for the theoretical flux PDF for different values of γ and referred to the case with $\gamma = -0.1$.
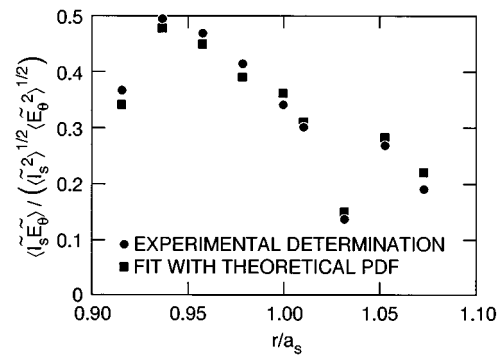

FIG. 15. Correlation parameter between ion saturation current fluctuations and poloidal electric field fluctuations as a function of the radius as measured in the TJ-I tokamak.

PDF of the duration of flux events at the edge of the sandpile. This PDF is also well described by a K_0 Bessel function. This result supports the previous result using the more detailed SOC transport model.

Therefore, the comparison of the local flux PDFs by themselves does not give a good criterion to distinguish between theoretical models. However, there are other distinguishing features related to the measurement of local fluxes as discussed in Ref. 26. Because in SOC models most transport is caused by large-scale avalanches, the most relevant distinction between models is in the different characteristic radial scale length associated with the flux as compared with the fluctuations. From this analysis, one concludes that it is necessary to compare correlations of fluxes at different radial positions to distinguish between these two types of theoretical models.

VI. RADIAL DEPENDENCE OF THE LOCAL FLUX PDF

As seen in Fig. 3, the local flux PDF presents a systematic variation as a function of the radial location. The results are for the TJ-I tokamak in the range $|r - a_s| < 1$ cm. This variation implies a decrease in the cross-correlation between density and poloidal electric field fluctuations as one moves toward the edge. We can see that effect by plotting the relative change of the theoretical PDF, Eq. (7), when the parameter γ changes. These plots are shown in Fig. 14, where we can see that the deviation of the PDF has a form similar to the one shown by the experimental results in Fig. 5. We have also calculated directly from the experimental results the correlation between ion saturation current and poloidal electric field fluctuations, showing the expected decrease as the radial position moves outwards (Fig. 15). The coherence obtained directly from the experiment [left-hand side of Eq. (10)] is compared with the value of γ obtained by fitting the PDFs [right-hand side of Eq. (10)]. This change of coherence also implies a change in the relative phase between density and potential fluctuations.

The theoretical models also give a radial dependence for the relative phase of density and poloidal electric field fluctuations. As can be seen in Fig. 16, there is a slow change in the phase, and superimposed on it is a sharp variation near the low-resonant surfaces. The slow change of phase is opposite to the one observed experimentally. However, the

theoretical calculation is for stellarator geometry and outside the range of the experiment, $|r - a_s| > 1$ cm. Therefore, no other conclusion can be drawn by this comparison except that of the possible relevance of low rational q surfaces in producing abrupt changes in the relative phase of the fluctuations.

The change of the PDF with radial position can also be quantified in terms of its skewness and kurtosis (Fig. 17). We can see that the values of both moments of the PDF are consistent with the predicted variation (Fig. 8). This finding gives us confidence that the values obtained are meaningful in spite of the accuracy problem. It is also consistent with an increase of γ as the probe moves inward in radius, as was obtained from the phase measurement (Fig. 15). This systematic change of the PDF with radial position being consistent with the change in skewness and kurtosis gives credibility to these results, in which statistical significance is often in question. The values of both skewness and kurtosis also agree well with the ones obtained from Eqs. (12) and (13) using γ from the fits to the PDF.

In the case of the TJ-IU, the variation of the relative phase between density and potential fluctuations with radius is not smooth. The phase dependence has radial structure with peaks (quasicoherent modes?) that could be related to
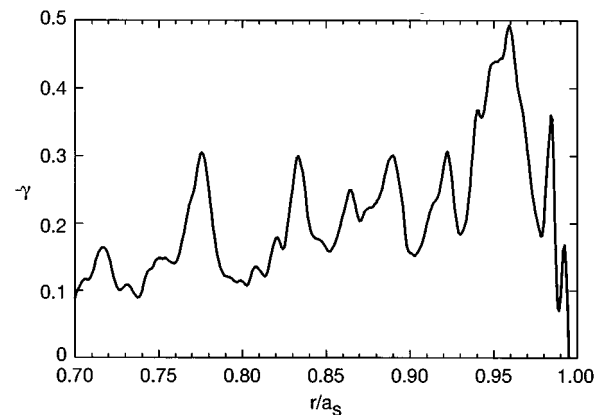

FIG. 16. Relative phase between the density and potential fluctuations as a function of the radius from the resistive pressure-gradient-driven turbulence model.

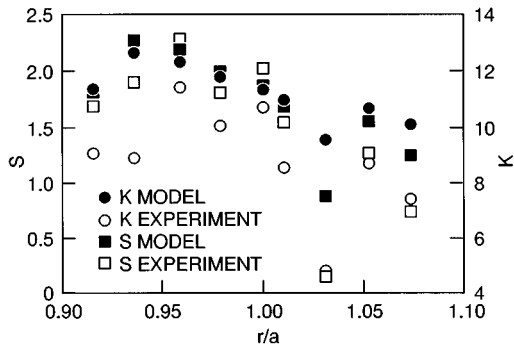2670 Phys. Plasmas, Vol. 3, No. 7, July 1996

Carreras *et al.*

FIG. 17. Radial dependence of the skewness and kurtosis of the flux distribution function in TJ-I tokamak compared with the values given by Eqs. (12) and (13) with γ obtained from fitting the experimental PDFs.

the existence of rational surface.[27] This type of structure is shown in results of the theoretical model (Fig. 16). This difference between TJ-I and TJ-IU could be attributed to the stellarator configuration versus the tokamak. In the stellarator, resistive interchange modes can be the relevant edge instability. These modes are localized near the lowest q resonances. However, in the case of the tokamak, the instability has a more ballooning character, and the fluctuations have smoother behavior near the singular surfaces. Another reason could be the low shear of the stellarator versus the higher shear of the tokamak. The magnetic shear dependence of the instability width could make the tokamak quasicoherent modes very narrow, below the radial resolution of present TJ-I experiments. This explanation would be consistent with the results from the TEXT tokamak.[28]

Both the ion saturation current and the floating potential signals have a nearly Gaussian distribution function in the edge region of the plasma ($r < a_s$). However, the I_s fluctuations systematically and increasingly deviate from the Gaussian distribution as the probe moves into the SOL region of the plasma. This change in the probability distribution function for I_s fluctuations is clearly observed by comparing the data measured at two different radial locations ($r/a_s \approx 1.05$ and $r/a_s \approx 0.95$) as shown in Fig. 18. This change does not
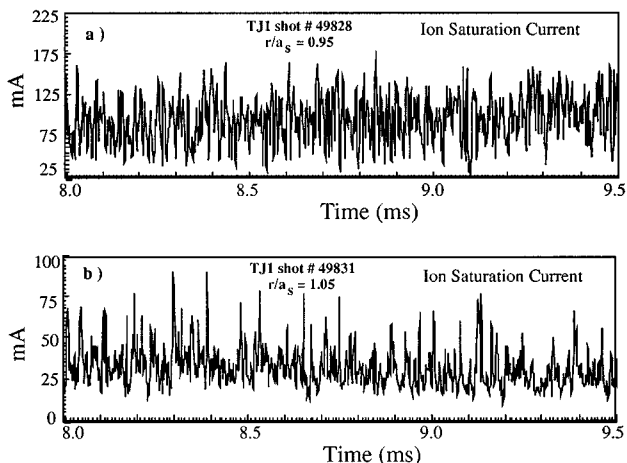

FIG. 18. Time evolution of I_s measured at (a) $r/a_s \approx 0.95$ and at (b) $r/a_s \approx 1.05$.
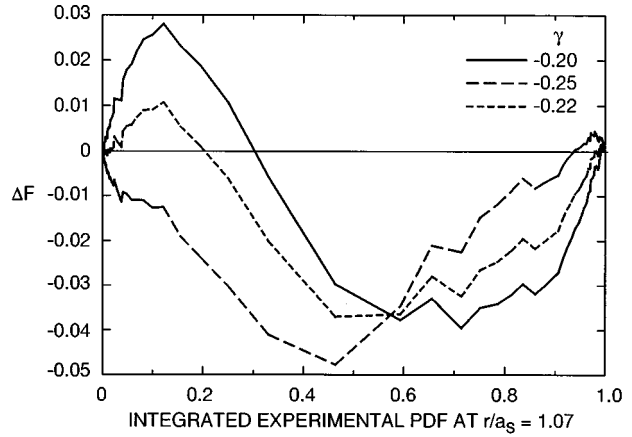

FIG. 19. Quantile–quantile plot for the experimental flux PDF at $r/a_s = 1.07$ referred to the theoretical expression given by Eq. (7) for three values of γ.

necessarily imply a change on the statistical nature of the fluctuations. As the mean value of the fluctuations increases relative to the averaged value, the Gaussian distribution function is not a good description for a variable that is positive definite. A Poisson-like distribution function could be more adequate. This is the case for I_s. In Fig. 1, we can see that the mean value of I_s decreases toward the plasma edge, while the fluctuations remain large. However, the electrostatic potential does not have the positivity restriction. Another possibility is the nonlinear nature of the saturation current. Since $I_s \propto n_e \sqrt{T_e}$, as the fluctuations increase, the fluctuating part of the saturation current must include the nonlinear coupling of density and temperature fluctuations. To this point, we have neglected the $\tilde{T}_e$ effects in I_s. Because there are edge fluctuation measurements done with the fast probes that allow the separation between the density and temperature fluctuations, we can plot the PDF for each type of fluctuation separately. In the SOL, both PDFs show a deviation from a Gaussian. Therefore, the most probable cause of the deviation of a Gaussian PDF is the positive definite nature of the density and temperature when the fluctuation components are close to their mean value.

Because the I_s fluctuation PDF deviates from Gaussian in the SOL, we cannot expect that Eq. (6) describes the local flux PDF in the SOL. Taking the results at $r/a_s = 1.07$, the best fit to the PDF is for $\gamma = -0.22$. However, when we check the theoretical PDF deviation from the experimental one, we observe a systematic discrepancy (Fig. 19). This fit also fails the Kolmogorov test, indicating that the functional form of the PDF given by Eq. (7) is no longer right but still gives a qualitative representation of the data.

VII. CONCLUSIONS

The measurements of the fluctuation-induced flux at the plasma edge indicate that the particle loss is intermittent and that the flux is bursty. This result is consistent with the quasi-Gaussian statistics of the density and electrostatic potential fluctuations, and it is not necessary to invoke non-Gaussian statistics to explain the bursty character of the fluxes. On the basis of Gaussian statistics, a simple expression for the tur-

bulent flux can be derived that agrees well with the experimental measurements. In separating systematic from statistical effects between different types of PDFs, the quantile–quantile plots have proven to be very useful.

The statistical properties of fluctuations and turbulent transport are different in the plasma bulk side and SOL side of the velocity shear layer in the TJ-I tokamak. The local flux PDF presents a systematic variation as a function of the radial location as a consequence of a decrease in the cross-correlation between density and potential fluctuations as one moves toward the edge.

The strong similarity in the statistical properties of the turbulent fluxes in the TJ-I and TJ-IU devices suggests a generic character of the plasma turbulence in magnetic confinement devices already observed in the comparison between ATF and TEXT plasmas. The present results emphasize the importance of comparative studies between the structure of plasma turbulence in tokamaks and stellarator plasmas to critically evaluated edge turbulence models. Further comparative studies would be desirable to test whether the similarities between tokamak and stellarator edge fluctuations reflect a universal character of edge turbulence.

Most theoretical models lead to Gaussian statistics for fluctuations. Even in the two extreme situations of comparing supercritical with subcritical transport, the fluxes have similar statistical distribution. Therefore, the comparison of the local flux PDFs by themselves does not give a good criterion to distinguish between theoretical models. As discussed elsewhere,[26] because in SOC models most transport is caused by large-scale avalanches, the most relevant distinction between models is in the different characteristic radial scale length associated with the flux as compared with the fluctuations. From this analysis one concludes that it is necessary to compare correlations of fluxes at different radial positions to distinguish between these two types of theoretical models.

ACKNOWLEDGMENTS

[1] Ch. P. Ritz, T. L. Rhodes, H. Lin, W. L. Rowan, H. Tsui, M. Meier, R. D. Bengston, A. J. Wootton, B. A. Carreras, J.-N. Leboeuf, D. K. Lee, J. H. Harris, C. Hidalgo, J. D. Bell, J. A. Holmes, R. C. Isler, V. E. Lynch, T. Uckan, P. H. Diamond, A. S. Ware, and D. R. Thayer, in *Plasma Physics and Controlled Nuclear Fusion Research*, Proceedings of the 13th International Conference, Washington, DC (International Atomic Energy Agency, Vienna, 1991), Vol. II, p. 589.

[2] Y. W. Tsui, A. J. Wootton, J. D. Bell, R. D. Bengston, D. Diebold, J. Harris, N. Hershkowitz, C. Hidalgo, J. C. Ingraham, S. J. Kilpatrick, G. X. Li, H. Lin, Ch. P. Ritz, A. Rudyj, K. F. Schoenberg, J. Soresen, T. Tanaka, T. Uckan, and P. G. Weber, Phys. Fluids B **5**, 2491 (1993).

[3] M. Endler, L. Giannone, K. McCormick, H. Niedermeuer, A. Rudyi, G. Theimer, N. Tsois, S. Zoletnik, the ASDEX Team, and the W7-AS Team, *Proceedings of the 21st EPS Conference on Controlled Fusion and Plasma Physics*, Montpellier (European Physical Society, Petit-Lancy, 1994), Vol. 18B, Pt. II, p. 874.

[4] G. Vayakis, Nucl. Fusion **33**, 547 (1992).

[5] L. Giannone, R. Balbín, H. Niedermeyer, M. Endler, G. Herre, C. Hidalgo, A. Rudyj, G. Theimer, Ph. Verplanke, and the W7-AS Team, Phys. Plasmas **1**, 3614 (1994).

[6] C. Hidalgo, J. H. Harris, T. Uckan, J. D. Bell, B. A. Carreras, J. L. Dunlap, G. R. Dyer, Ch. P. Ritz, A. J. Wootton, M. A. Meier, T. L. Rhodes, and K. Carter, Nucl. Fusion **31**, 1471 (1991).

[7] J. F. Lyon, B. A. Carreras, K. K. Chipley, M. J. Cole, J. H. Harris, T. C. Jernigan, R. L. Johnson, V. E. Lynch, B. E. Nelson, J. A. Rome, J. Sheffield, and P. B. Thompson, Fusion Technol. **10**, 179 (1986).

[8] K. W. Gentle, Nucl. Technol./Fusion **1**, 479 (1981).

[9] ASDEX Team, Nucl. Fusion **29**, 1959 (1989).

[10] M. Keilhacker and the ASDEX Team, Nucl. Fusion **25**, 1045 (1985).

[11] H. Renner, the WII-AS Team, the NBI Group, the ICF Group, and the ECRH Group, Plasma Phys. Controlled Fusion **31**, 1579 (1989).

[12] C. Hidalgo, Plasma Phys. Controlled Fusion **37**, A53 (1995).

[13] I. García-Cortés, M. A. Pedrosa, C. Hidalgo, B. Brañas, T. Estrada, R. Balbin, E. de la Luna, J. Sanchez, and A. P. Navarro, Phys. Fluids B **4**, 4007 (1992).

[14] E. Ascasibar, C. Alejaldre, J. Alonso, F. de Aragon, R. Balbin, B. Brañas, E. de la Cal, F. Castejon, J. Castrejon, G. Catalan, J. R. Cepero, T. Estrada, R. Fernandez, M. Frances, J. de la Gama, L. Garcia Gonzalo, I. Garcia Cortes, G. Gomez, J. Guasp, J. Herranz, C. Hidalgo, J. A. Jimenez Aparicio, A. Jimenez, V. Krivenski, I. Labrador, F. Lapayese, M. Liniers, A. Lopez Fraguas, J. Lopez Razola, A. Lopez Sanchez, E. de la Luna, R. Martin Garcia, E. Martin Roquero, L. M. Martinez, F. Medina, M. Medrano, B. P. van Milligen, M. A. Ochando, P. Ortiz, L. Pacios, L. Pallas, I. Pastor, M. A. Pedrosa, J. Qin, M. C. Rodriguez Fernandez, L. Rodrigo Rodrigo, F. Rufino, A. Salas, L. Sanchez Cabezudo, A. Sanchez Corpas, E. Sanchez Gonzalez, J. Sanchez Sanz, C. Sierra, F. Tabares, D. Tafalla, V. Tribaldos, A. Varias, J. Vega, B. Zurro, L. M. Kovrizhnykh, D. C. Akulina, O. F. Fedyanin, L. V. Kolik, K. M. Likin, Yu. I. Nechaev, A. E. Petrov, K. A. Sarksyan, N. V. Matveev, B. M. Rassadin, and E. M. Tai, "Initial operation of the TJ-IU torsatron," in *Plasma Physics and Controlled Fusion Research*, Proceedings of the 15th Conference on Plasma Physics and Controlled Nuclear Fusion Research, Seville (International Atomic Energy Agency, Vienna, in press).

[15] C. Hidalgo, R. Balbín, M. A. Pedrosa, I. Garcia-Cortes, and M. A. Ochanodo, Phys. Rev. Lett. **69**, 1205 (1992).

[16] M. Endler, H. Niedermeyer, L. Giannone, E. Holzhauer, A. Rudyj, G. Theimer, N. Tsois, and the ASDEX Team, Nucl. Fusion **35**, 1307 (1995).

[17] T. Huld, A. H. Nielsen, H. L. Pécseli, and J. Juul Rasmussen, Phys. Fluids B **3**, 1609 (1991).

[18] W. J. Conover, *Practical Nonparametric Statistics* (Wiley, New York, 1980).

[19] V. E. Lynch, B. A. Carreras, J. N. Leboeuf, D. E. Newman, and L. Garcia, Buffer **19**, 5 (1995).

[20] B. A. Carreras, L. Garcia, and P. H. Diamond, Phys. Fluids **30**, 1388 (1987).

[21] L. Garcia, H. R. Hicks, B. A. Carreras, L. A. Charlton, and J. A. Holmes, J. Comput. Phys. **65**, 253 (1986).

[22] L. A. Charlton, J. N. Leboeuf, B. A. Carreras, and V. E. Lynch, Phys. Plasmas **1**, 3871 (1994).

[23] B. A. Carreras, V. E. Lynch, L. Garcia, and P. H. Diamond, Phys. Plasmas **2**, 2744 (1995).

[24] P. Bak, C. Tang, and K. Weisenfeld, Phys. Rev. Lett. **59**, 381 (1987).

[25] P. H. Diamond and T. S. Hahm, Phys. Plasmas **2**, 3640 (1995).

[26] D. E. Newman, B. A. Carreras, P. H. Diamond, and T. S. Hahm, Phys. Plasmas **3**, 1858 (1996).

[27] M. A. Pedrosa, M. A. Ochando, J. A. Jiménez, R. Balbín, J. Qin, and C. Hidalgo, "Magnetic Configuration Effects on the TJ-IU Torsatron Plasma Edge," Plasma Phys. Controlled Fusion (1996) (in press).

[28] H. Tsui, K. Rypdal, Ch. Ritz, and A. Wootton, Phys. Rev. Lett. **70**, 2565 (1993).